Accepted by Physica C (Nov. 18, 2005)

ENHANCED CRITICAL CURRENT DENSITY OF $YBa_2Cu_3O_x$ FILMS GROWN ON $Nd_{1/3}Eu_{1/3}Gd_{1/3}Ba_2Cu_3O_x$ WITH NANO-UNDULATED SURFACE MORPHOLOGY

R. L. Meng[1], T. H. Johansen[1,2], I. A. Rusakova[1], A. Baikalov[1], D. Pham[1], F. Chen[1], Z. Y. Zuo[1] and C. W. Chu[1,3,4]

[1]*Department of Physics and the Texas Center for Superconductivity, University of Houston, Houston TX 77204-5002*

[2]*Department of Physics, University of Oslo, Box 1048 Blindern, N-0316 Oslo, Norway*

[3]*Lawrence Berkeley National Laboratory, 1 Cyclotron Road, Berkeley, CA 94720*

[4]*Hong Kong University of Science and Technology, Clear Water Bay, Kowloon, Hong Kong*

ABSTRACT

We report a simple and easily controllable method where a nano-undulated surface morphology of superconducting $Nd_{1/3}Eu_{1/3}Gd_{1/3}Ba_2Cu_3O_x$ (NEG) films leads to a substantial increase in the critical current density in superconducting $YBa_2Cu_3O_x$ (YBCO) films deposited by pulsed laser deposition on such NEG layers. The enhancement is observed over a wide range of fields and temperatures. Transmission electron microscopy shows that such YBCO films possess a high density of localized areas, typically 20×20 nm^2 in size, where distortion of atomic planes give rotational (2 to 5°) moiré patterns. Their distribution is random and uniform, and expected to be the origin of the enhanced flux pinning. Magneto-optical imaging shows that these films have excellent macroscopic magnetic uniformity.

PACS: 74.78.Bz
KEYWORDS: flux pinning, critical current density

INTRODUCTION

Practical applications of high temperature superconductor films depend crucially upon finding ways to enhance the flux pinning and thereby increase the critical current density, j_c, especially at high magnetic fields. Recent reports have shown that pre-decoration of the substrate by a high density of non-superconducting nano-sized particles is an efficient way of creating large numbers of strong pinning sites in the superconducting film that is subsequently deposited on the decorated surface. The basic idea of the method is using the nano particles to create a substantial lattice mismatch or chemical poisoning so that locally the superconducting phase is prevented from forming. Successful examples of this are sputtering nano-dots of Ag on a $SrTiO_3$ (STO) substrate prior to deposition of (Cu,Tl)$BaSrCa_2Cu_3O_y$, and pulsed laser deposition of nano-islands of Y_2O_3 and Ag on STO and YSZ substrates, respectively, prior to deposition of $YBa_2Cu_3O_x$ (YBCO).[1-4] In principle, the method can be extended by repeating the double deposition, as was demonstrated with alternating growth of an ultra thin layer of second-phase Y_2BaCuO_5 or Y_2O_3 and superconducting YBCO repeated up to 200 times.[5-6]

In this work we report a new and efficient method to obtain enhanced pinning in films of YBCO. The method is based on our observation that thin films of the mixed rare-earth compound $Nd_{1/3}Eu_{1/3}Gd_{1/3}Ba_2Cu_3O_x$ (NEG) grown by laser ablation on STO substrates develop a surface morphology with densely packed and sharply separated submicron-sized growth islands. We show that by using such a nano-undulated surface as a sublayer for deposition of YBCO films, one obtains an increase in j_c of approximately 50%. Magneto-optical (MO) imaging studies reveal that such YBCO films have excellent

uniformity and are therefore well suited for device applications. Moreover, since the NEG sublayer itself is superconducting, the method also gives a high engineering j_c.

EXPERIMENTAL

The YBCO and NEG films were deposited by pulsed laser deposition on $SrTiO_3$ (001) single-crystal substrates. Targets of NEG were prepared with stoichiometric R_2O_3 (R = Nd, Eu, Gd), $BaCO_3$, and CuO powders sintered at 950 °C. X-ray diffraction confirmed that the target consists of pure 123 phases. Before deposition the substrates were cleaned by heating to 900 °C for 30 minutes. The films were deposited at a temperature of 810 – 830 °C in a 350 mTorr oxygen atmosphere using a KrF excimer laser with RF power of 250 mJ.

In synthesizing the two-layer films the deposition of YBCO and NEG was done in the same process. We found that optimal conditions for YBCO deposition is to use the same oxygen pressure and laser energy as for NEG, and lowering the deposition temperature close to 800 °C. After deposition, the films were in-situ annealed at 450 – 500 °C, maintaining the oxygen pressure for 30 minutes, before cooling down to room temperature. No *ex situ* annealing was employed. Note that the synthesis of the two films in the proper order is possible because the melting point of NEG is the higher of the two compounds.

For comparison, films of YBCO were also deposited directly on STO substrates using the same conditions. Transport measurements showed a transition temperature of 92 K for

the YBCO films. The film thickness was measured using α-step surface profilometry. The surface morphology was studied using an Explorer Atomic Force Microscope (AFM).

The critical current density was investigated by magneto optical (MO) imaging using in-plane magnetized bismuth-substituted iron-garnet films as an indicator. The setup consists of an Olympus polarizing microscope and an Oxford Microstat-He optical cryostat with a custom-made coil to apply an external magnetic field. We used a fully crossed polarizer and analyzer setting, giving images where the brightness represents the magnitude of the local flux density. The field dependence of j_c was measured in the field range from zero and up to 5 T using a SQUID magnetometer. The microstructure was investigated by transmission electron microscopy (TEM) using a JEOL 2000FX microscope operated at 200 kV. Cross-sectional samples were prepared by a standard procedure and ion milling was carried out with 4 keV Ar ions.

RESULTS AND DISCUSSION

Shown in Fig. 1 are the surface morphologies of a typical bare NEG film observed using atomic force microscopy (AFM). This 100 nm thick film is densely packed with growth islands, resulting in an undulated surface having a highly uniform and narrow distribution of peaks 15 – 25 nm high and 80 – 100 nm in diameter (Fig. 1b). This type of surface morphology is similar to that reported by Cai et al.[7], except that there are CuO, BaO or BaCuO droplets due to the fact that we did not employ off-axis deposition (Fig. 1b). The AFM results are also in good agreement with Cai et al quantitatively. In comparison, Fig.

2 shows typical bare YBCO surface morphology by AFM, which clearly lacks the mono-dispersed nano-undulations. We therefore expect that the nano-undulation on the NEG film may introduce additional pinning centers for YBCO deposited on top of it, thus the multi-layered films YBCO/NEG/STO are grown and tested. The droplets of Cu and Ba oxides have relative low density and large size, thus should not have significant influence on the pinning properties.

Fig. 3 shows an MO image of YBCO/NEG samples with layer thicknesses of 100 nm and 50 nm, respectively. The image was taken at 5 K in an applied field of B_a = 45 mT. As seen directly from the image, the two-layer film has excellent uniformity in superconducting properties on the macroscopic scale. Only one defect in the upper half of the film is visible, as it creates a parabolic fan-like flux pattern starting from a point inside the strip. Since the superconducting film covers the whole substrate area, a slight edge roughness is also causing fan-like flux structures, which can be seen starting from both the upper and lower edges in the image.

From MO images the low-field critical current density was determined from the Bean model formula for a long thin strip, $\mu_0 J_c = \pi B_a / \cosh^{-1}(w/a)$, where J_c is the sheet current (the current density integrated over the film thickness), and a and w are the width of the central flux free area and the width of the strip itself, respectively. Since these samples consist of two different superconducting layers, the sheet current has two contributions: $J_c = j_c\, d + j_c^{\mathrm{NEG}}\, d^{\mathrm{NEG}}$, where j_c and d are the critical current density and thickness of the YBCO layer, and where the second term represents the current flowing

in the NEG layer. We determined j_c^{NEG} from MO images of flux penetration in bare NEG films prepared under the same deposition conditions. The current density in this layer was not very high, *e.g.* $j_c^{NEG}(5\ K) = 0.7 \cdot 10^7\ A/cm^2$; however, optimizing the critical current in the NEG film is not the focus of the present work. Using the procedure described above, we find for the YBCO layer alone that $j_c = 7.1 \cdot 10^7\ A/cm^2$ at 5 K. At higher temperatures, we obtain the values listed in the Table 1. Also included in the table are j_c values measured on a reference YBCO/STO sample grown under the same conditions. We find consistently that YBCO on NEG gives an enhancement in j_c of 50% - 100% between 5 K and 77 K.

The field dependence of the j_c results are plotted in Fig. 4, where full symbols show j_c of YBCO on NEG, and open symbols represent YBCO/STO. For the two-layer film, j_c of the YBCO part was extracted using that in fully penetrated states the measured magnetic moment equals $m = (j_c d + j_c^{NEG} d^{NEG}) \times$ geometrical factor, where the second factor is given by the sides of the rectangular sample used for the SQUID measurements. The results clearly show that the field behavior of the YBCO film is also largely improved by the NEG sublayer. Over the whole field range, j_c is increased by 40 – 50 % both at 5 K and 45 K. Note that the zero-field j_c obtained from the M-H loop width is slightly lower than the values obtained from MOI, which is to be expected as explained in Ref. 8.

To clarify the origin of this pinning enhancement, the samples were investigated by transmission electron microscopy (TEM). Fig. 5a shows a TEM bright-field image of a double-layer film obtained under mass-thickness contrast image formation conditions.

This type of contrast arises from incoherent (Rutherford) elastic scattering of electrons, which is a strong function of atomic number Z. The difference between the Y ions (Z = 39) in the upper YBCO film and the much heavier ions of Nd, Eu, and Gd (Z = 60, 63, and 64, respectively) in the sublayer results in a clear contrast between the two films. Their interface has a very distinct wavy appearance, which is in full quantitative agreement both in inter-peak distance and in undulation amplitude with the AFM image obtained for the bare NEG film. We conclude therefore that its surface morphology remains intact throughout the deposition of the YBCO film. Note also from the TEM image that both the NEG/STO and the YBCO/NEG interfaces are uniform. Moreover, selected area electron diffraction (SAED) recorded from the substrate and the two layers shows that both films are very well c-axis aligned with the substrate (see Fig. 5c).

Shown in Fig. 5b is the microstructure of the double-layer film obtained by conventional bright-field TEM revealing strain contrast. While the NEG/STO shows strain mainly along the interface, the YBCO layer contains numerous strained regions throughout its volume. Mismatch of lattice parameters on both interfaces is about the same, and it is less than 1%.This strongly suggests that the strained regions inside the YBCO film stem from the interface undulation. Indeed, high resolution TEM (see Fig. 4d), reveals that in the YBCO layer, strained regions start from the interface. Moreover, we find that locally the atomic planes have orientation deviations from 2 to 5°, resulting in rotational moiré patterns, four of them shown by arrows. Moiré patterns reveal that size of distortion is very small, typically 20×20 nm^2, and they are randomly and quite uniformly distributed. Such occurrence of distortions is unique compared to other YBCO films deposited on

different substrates. We would like to point out that the distance between the areas showing rotational moiré patterns is in the range of s = 10-50 nm. Assuming that they are responsible for the additional flux pinning, this high density is fully capable of producing the considerable enhancement of j_c over a wide range of fields. The matching field, $B \sim \Phi_0/s^2$, corresponding to each extra pinning site (moiré area) being occupied by one flux quantum Φ_0, covers a range up to several Tesla. This means that in the field interval where we have made magnetic measurements one should expect considerable pinning enhancement, and thereby contributing largely to the enhancement of the critical current density in our YBCO films. Additional contributions can come from the high density of stacking faults, and therefore partial dislocations, which are also found to be present in the YBCO layer of YBCO/NEG/STO as confirmed by SAED patterns (Fig. 6a). Streaks from stacking faults are observed on diffraction pattern from the YBCO film (Fig. 6a) while the diffraction pattern from NEG film is almost streak-free (Fig. 6b). For comparison, the diffraction pattern from YBCO/STO (Fig. 6c) shows the presence of streaks caused by stacking faults but with a much lower density than in the YBCO/NEG/STO film.

In conclusion, we have demonstrated that a nano-undulated surface morphology of superconducting NEG films leads to a substantial increase in the critical current density in YBCO films deposited on top of the NEG layer. The enhancement is observed over a wide range of fields and temperatures. Compared to most other methods of non-superconducting nano-patterning of substrates, this new method is technologically simple, easily controllable, and economically favorable, which will lead to higher

engineering critical current density, particularly if the NEG layer is optimized. Because the pinning centers may not persist when the top YBCO film gets thicker, an interesting extension of this work would be to make a periodic multilayer structure YBCO/NEG/…/YBCO/NEG/STO to provide films with large total critical current with thicker films.

ACKNOWLEDGMENTS

We thank Y.Y. Sun for X-ray analysis of the samples. The work at Houston is supported in part by NSF Grant DMR-9804325, the T. L. L. Temple Foundation, the John and Rebecca Moores Endowment, and the State of Texas through the Texas Center for Superconductivity at the University of Houston; and at Lawrence Berkeley Laboratory by the Director, Office of Science, Office of Basic Energy Sciences, Division of Materials Sciences and Engineering of the U.S. Department of Energy under Contract No. DE-AC03-76SF00098. One of the authors (THJ) is grateful to the Norwegian Research Council for financial support.

REFERENCES

1. A. Crisan, S. Fujiwara, J.C. Nie, A. Sundaresan and H. Ihara, Appl. Phys. Lett. **79**, 4547 (2001).

2. K. Matsumoto, T. Horide, K. Osamura, M. Mukaida, Y. Yoshida, A. Ichinose, S. Horii, Physica C **412-414**, 1267 (2004).

3. D.B. Jan, Q.X. Jia, M.E. Hawley, G.W. Browne, C.J. Wetteland, H.P Sun, X.P. Pan, J. Mater. Res. **17**, 697 (2000).

4. M. Ionescu, A.H. Li, Y. Zhao, H.K. Liu and A. Crisan, J. Phys. D: Appl. Phys. **37**, 1824 (2004).

5. T. Haugan, P.N. Barnes, R. Wheeler, F. Meisenkothen and M. Sumption, Nature **430**, 867 (2004).

6. T.A. Campbell, T.J. Haugan, I. Maartense, J. Murphy, L. Brunke, P.N. Barnes, Physica C **423**, 1 (2005).

7. C. Cai, B. Holzapfel, J. Hänisch, L. Fernandez and L. Schultz, Phys. Rev. B **69**, 104531 (2004).

8. D. V. Shantsev, Y. M. Galperin and T. H. Johansen, Phys. Rev. B **61**, 9699 (2000).

FIGURE CAPTIONS

Fig. 1 AFM images of surface areas of an NEG film deposited on STO, serving as sub-layer for subsequent deposition of a YBCO film. (a) Droplets of CuO, BaO or BaCuO as observed in 80×80 μm^2 scale. (b) The NEG growth granules with diameters of 80-100 nm and heights of 20-25 nm appear nearly mono-disperse in 5×5 μm^2 scale.

Fig 2 AFM image of a 5×5 μm^2 surface area of a YBCO film deposited on STO substrate showing no nano-granules as observed in NEG film.

Fig. 3 MO image of flux penetration in a two-layer YBCO/NEG film. The image was recorded at 5 K in a perpendicular applied field of 45 mT, and shows the strip-shaped sample in a partially penetrated state. The dark central band is the Meissner state part of the film, and the field exclusion causes the enhanced brightness seen along the film edge. The strip width is 3 mm.

Fig. 4 Critical current density in YBCO films as a function of applied magnetic field. The solid symbols represent YBCO/NEG (100nm/50nm) film, and open symbols show 100nm YBCO on the bare STO substrate.

Fig. 5 (a) TEM image of the two-layer film cross section taken under mass contrast imaging conditions. (b) Conventional TEM bright-field image of the interface. In both panels, the arrow points at the undulated YBCO/NEG interface. (c) Selected area diffractogram representing the full YBCO/NEG/STO structure. (d) High resolution TEM of the YBCO layer showing several areas (see arrows) with rotational moiré patterns.

Fig 6 SAED patterns from (a) YBCO layer of YBCO/NEG/STO, (b) NEG layer/STO

and (c) YBCO/STO.

TABLE 1

The table shows j_c in units of 10^7 A/cm^2 for the YBCO/NEG (100nm/50nm) film at different temperatures. Also shown is the j_c of a reference 100nm YBCO film.

	5 K	60 K	77 K
YBCO/NEG/STO	7.2	1.8	0.46
YBCO/STO	4.7	1.2	0.24

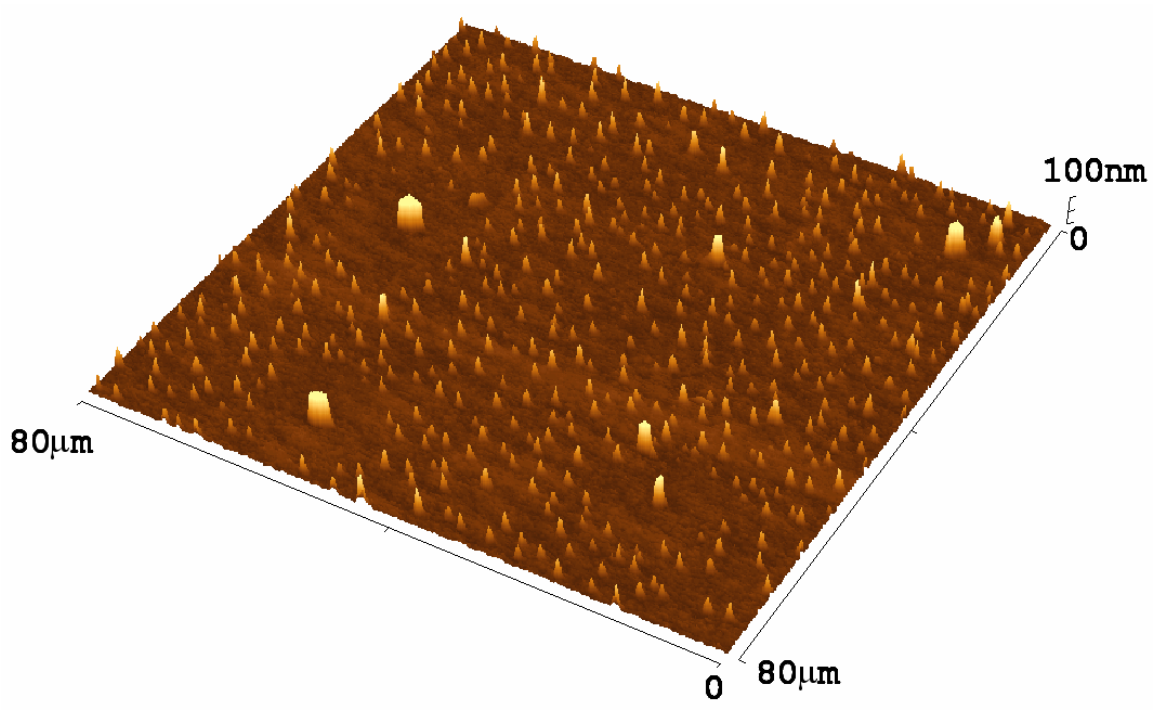

Fig. 1a
R. L. Meng et. al.

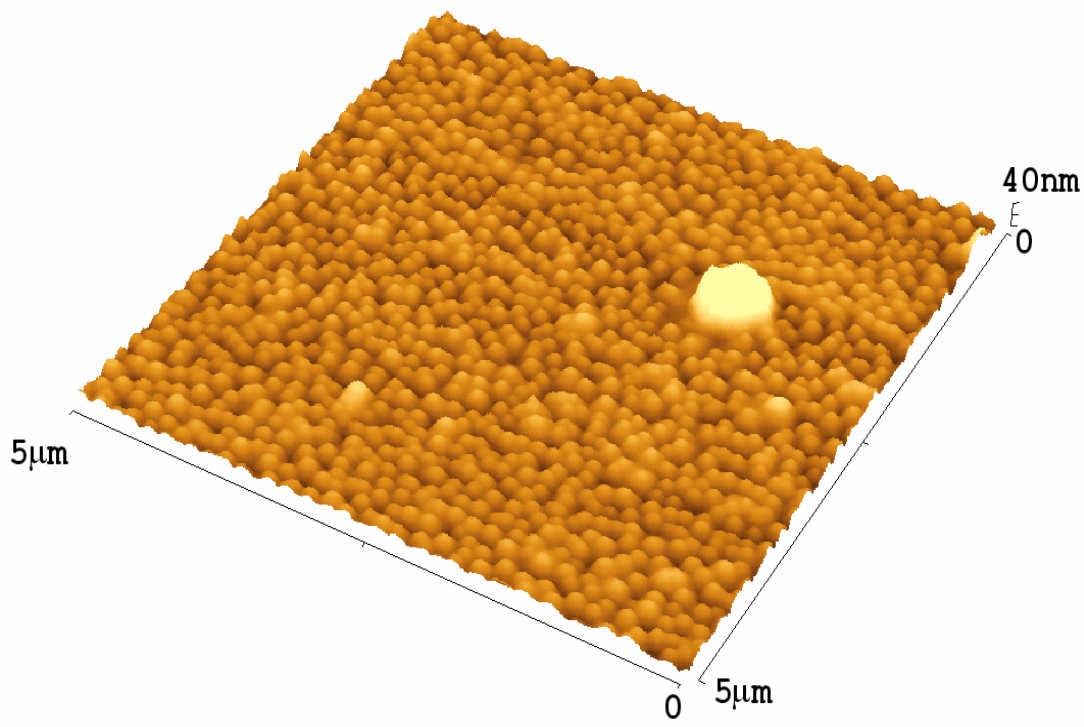

Fig. 1b
R. L. Meng et. al.

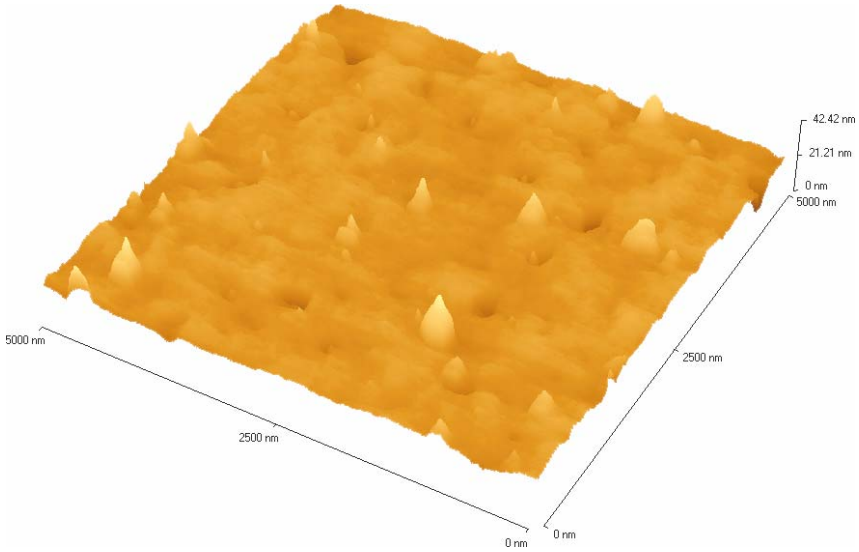

Fig. 2
R. L. Meng et. al.

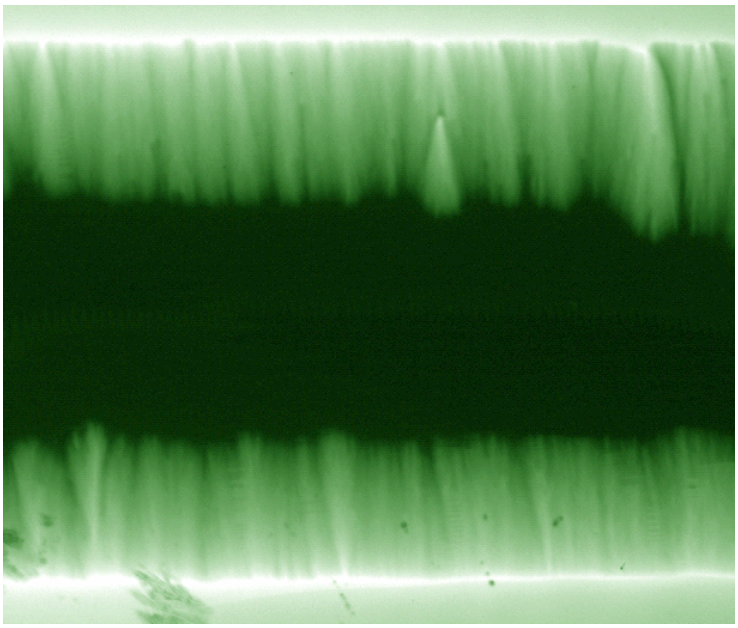

Fig. 3
R. L. Meng et. al.

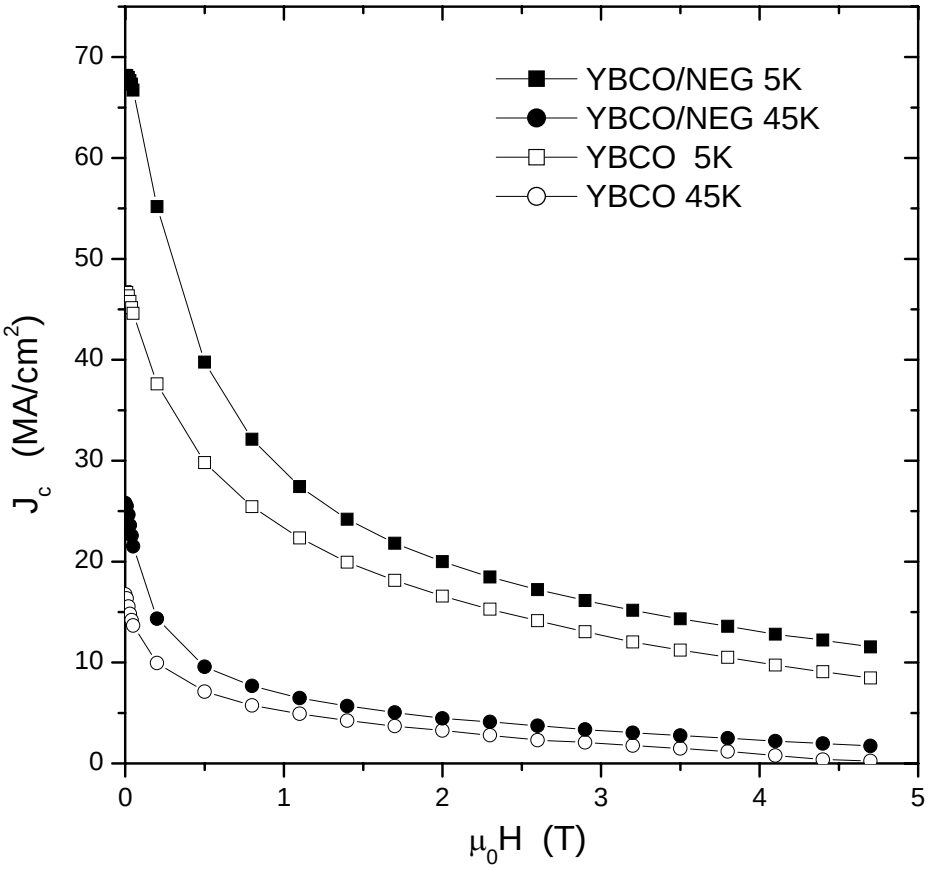

Fig. 4
R. L. Meng et. al.

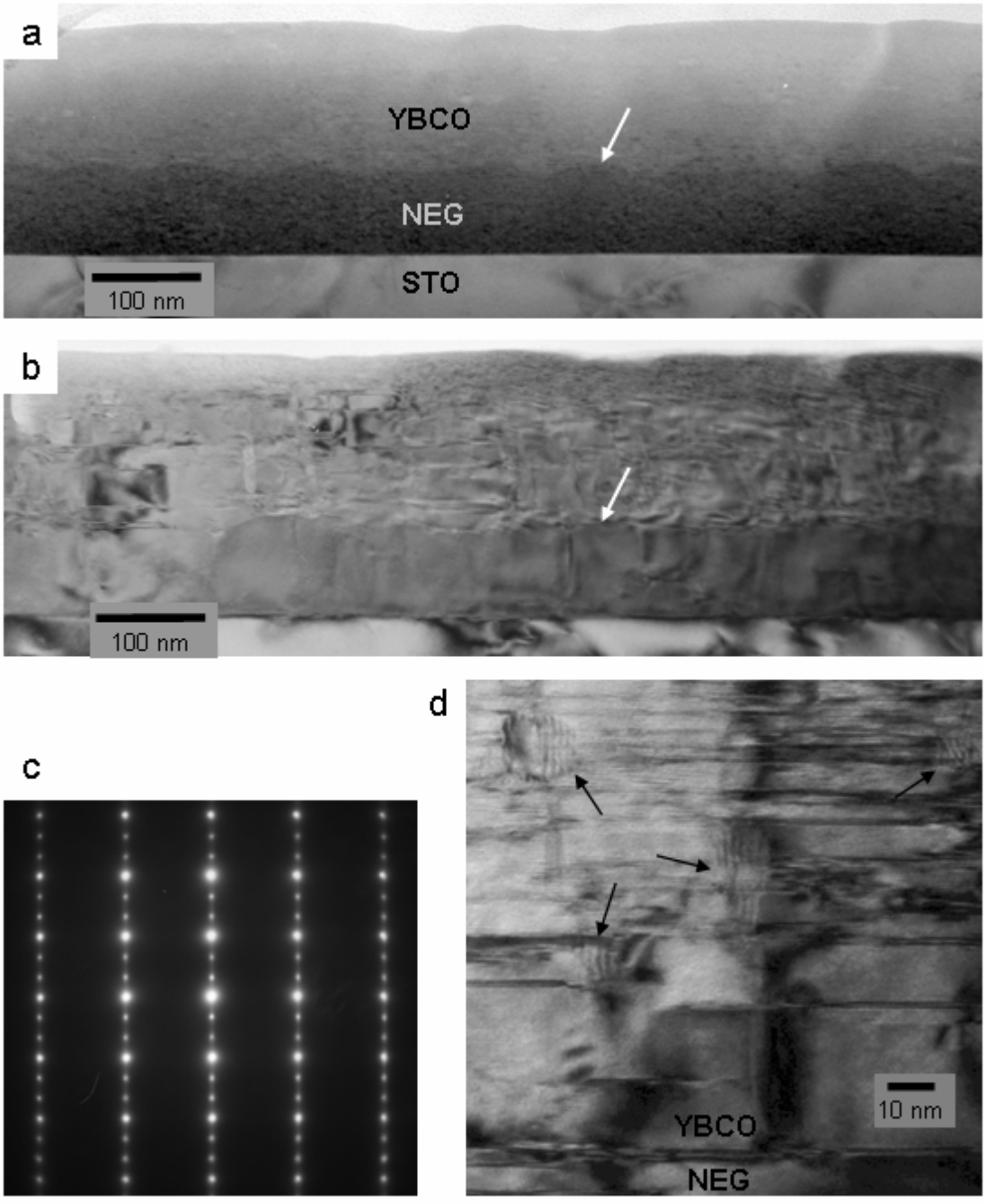

Fig. 5
R. L. Meng et

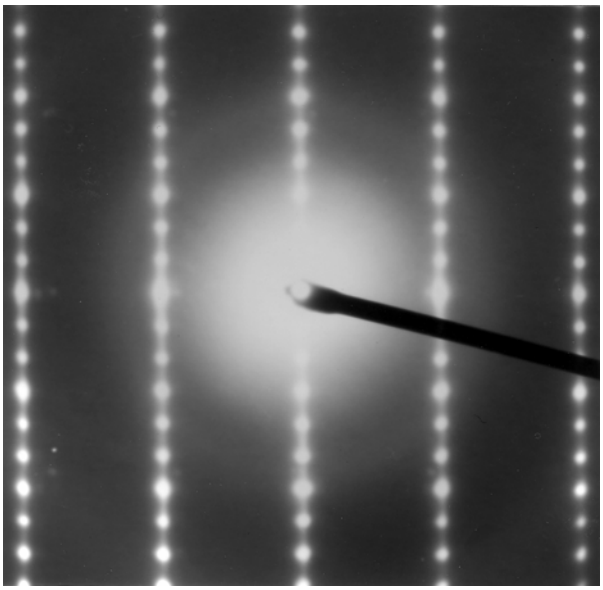

Fig. 6a
R. L. Meng et. al.

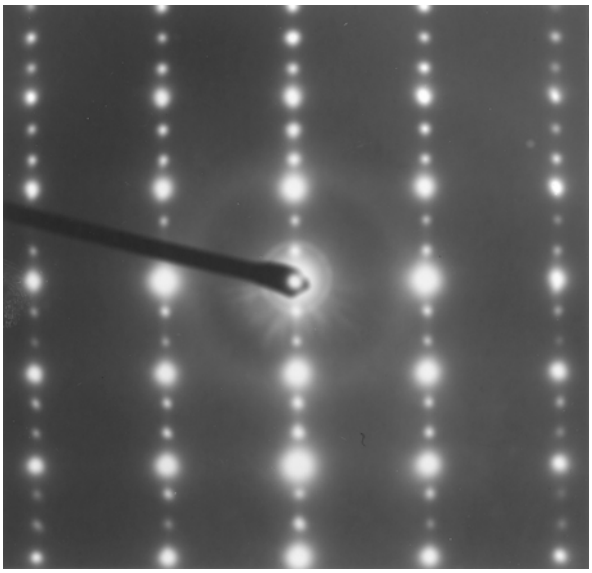

Fig. 6b
R. L. Meng et. al.

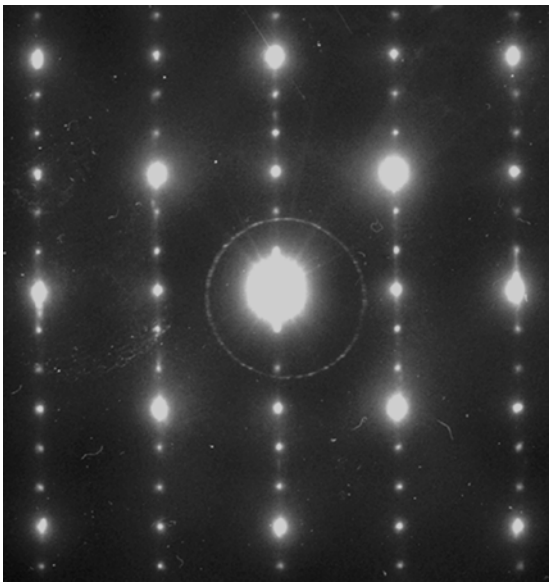

Fig. 6c
R. L. Meng et. al.